



The role of sphingomyelin in regulating phase coexistence in complex lipid model membranes: Competition between ceramide and cholesterol

Galya Staneva^{a,*}, Claude Chachaty^b, Claude Wolf^b, Kamen Koumanov^a, Peter J. Quinn^{c,*}

^a Institute of Biophysics, Bulgarian Academy of Sciences, Acad. G. Bonchev Str., Bl.21, 1113 Sofia, Bulgaria

^b Université Paris 6, INSERM U538, CHU St. Antoine, 27 rue Chaligny, 75012 Paris, France

^c Biochemistry Department, King's College London, 150 Stamford Street, London SE1 9NH, UK

ARTICLE INFO

Article history:

Received 16 May 2008

Received in revised form 14 July 2008

Accepted 28 July 2008

Available online 5 August 2008

Keywords:

Ceramide

Cholesterol

Sphingomyelin

Lipid signaling pathways

ABSTRACT

The structure, thermotropic phase behavior, dynamic motion and order parameters of bilayer dispersions of egg phosphatidylcholine, egg sphingomyelin, egg ceramide and cholesterol have been determined. The coexistence of gel, liquid-ordered and liquid-disordered structure has been determined by peak fitting analysis of synchrotron X-ray powder patterns. Order parameters and extent of distribution of 16-doxyl-stearic acid spin probe between ordered and disordered environments has been estimated by ESR spectral simulation methods. The presence of ceramide in proportions up to 20 mol% in phosphatidylcholine is characterized by gel–fluid phase coexistence at temperatures up to 46 °C depending on the amount of ceramide. Cholesterol tends to destabilize the ceramide-rich domains formed in phosphatidylcholine while sphingomyelin, by formation of stable complexes with ceramide, tends to stabilize these domains. The stability of sphingomyelin–ceramide complexes is evident from the persistence of highly ordered structure probed by ESR spectroscopy and appearance of a sharp wide-angle X-ray reflection at temperatures higher than the gel–fluid transition of ceramide alone in egg phosphatidylcholine bilayers. The competition between ceramide and cholesterol for interaction with sphingomyelin is discussed in terms of control of lipid-mediated signaling pathways by sphingomyelinase and phospholipase A₂.

Crown Copyright © 2008 Published by Elsevier B.V. All rights reserved.

1. Introduction

In the recent years many studies have been devoted to the role of sphingolipids in the formation and organization of “raft” microdomains [1–3]. The essential feature of these domains is that they are created by an association of particular molecular species of membrane lipids that are more ordered than the surrounding lipids of the fluid bilayer matrix. While the participation of sphingomyelin (SM) and glycosphingolipids in these domains is well established, the role of ceramides (CER) is not so clear.

Ceramides are relatively minor lipid components of cell membranes, varying between 1 and 10% in proportion to the glycerophospholipids [4]. Despite being minor constituents they are known to be mediators of vital cellular processes such as apoptosis, aging, differentiation, cell growth etc.[5–7]. The molecular mechanism that underlies the action of ceramides is to modulate the activity of particular enzymes. One example that we have demonstrated is the action of ceramide as an activator of secretory and cytosolic phospholipase A₂ (PLA₂) [8]. It was suggested that enzyme activation was

accomplished by the ability of ceramide to form microdomains and membrane defects in the substrate bilayer created by the juxtaposition of liquid-crystalline and gel phases. Such topological features are known to be recognised by antibodies [9]. Similar studies of the activation of phospholipase enzymes have subsequently confirmed these initial findings [10].

Cellular ceramides are generated both by *de novo* synthesis [11] and as products of hydrolysis of SM by various sphingomyelinases [12]. Levade and co-workers [13] showed that membrane sphingomyelinase is localized in raft domains inferring that CER generation takes place in the raft domains [14,15].

CER and SM differ in their affinity to interact with other lipids that make up the membrane bilayer matrix especially cholesterol (CHOL). SM interacts with CHOL to create a liquid-ordered structure, whereas CER shows a relatively weak affinity towards CHOL. Moreover, CER exhibits a tendency to segregate into domains highly enriched in CER [16–18]. This has been observed in giant unilamellar vesicles (GUV) in which ceramide-enriched microdomains were rapidly formed after treatment of vesicles comprised of phosphatidylcholine/sphingomyelin with sphingomyelinase [19]. One of the results of ceramide accumulation is that small vesicles budd off from the GUV. The mediation of vesicle budding by ceramide is known to be a mechanism for sorting subcellular membrane into different populations of intracellular vesicles [20].

* Corresponding authors. G. Staneva is to be contacted at tel.: +33 140011490; fax: +33 3140011499. P.J. Quinn, tel.: +44 2078484408; fax: +44 2078484500.

E-mail addresses: gstaneva@obzor.bio21.bas.bg (G. Staneva), p.quinn@kcl.ac.uk (P.J. Quinn).

CER possesses a chemical structure that is distinct from the other polar lipids of the membrane. They are characterized by a small polar headgroup and they have a strong tendency to self-assemble. The resulting structures display strong intermolecular interactions mediated by intermolecular hydrogen bonds. These cohesive forces operating within the compact arrangement created in CER-enriched domains produce a high order-disorder phase transition temperature, well above physiological temperatures [21]. Ceramides enhance the ordering of acyl chains in lipid bilayers and tend to stabilize the gel phase [22]. In addition, CER have been reported to incorporate preferentially into liquid-ordered domains and to displace CHOL associated with SM in membrane lipid rafts [23]. The same authors also showed that ceramides have a higher affinity towards lipid bilayers compared to CHOL. Thus CER and CHOL compete in their association with lipid rafts because of the limited capacity of the glycerophospholipids present in the raft domains to shield their small polar groups from contact with water [24,25].

Sphingomyelin is known to interact with cholesterol to form liquid-ordered phase and this interaction competes with the binding of sphingomyelin with both ceramide and intrinsic membrane proteins in biological membranes [26]. This dynamic property of sphingomyelin is the reason for its pivotal role in lipid ordering in the outer leaflet of resting cell membranes. Hydrolysis of sphingomyelin in GUVs comprised of phosphatidylcholine/sphingomyelin and cholesterol by bacterial sphingomyelinase leads to a progressive disappearance of raft domains [27,28]. Apparently, SM hydrolysis and CER accumulation are not conducive to raft stabilization. In the present study we have investigated competition of cholesterol and ceramide in bilayers containing sphingomyelin. X-ray diffraction methods have been used to characterize bilayer structure and thermotropic phase behavior and ESR spectroscopic probe methods have been used to provide information on lipid dynamics and order.

2. Materials and methods

2.1. Lipids

Egg sphingomyelin (ESM), egg phosphatidylcholine (EPC), egg ceramide (ECER) and cholesterol were purchased from Sigma (Sigma-Aldrich, St. Quentin-Fallavier, France). The fatty acid composition of EPC and ESM was examined by gas chromatography/mass spectrometry to confirm the absence of detectible fatty acid degradation after exposure to the synchrotron X-ray beam. ESM is mostly amidified with C16:0 (68%) and C18:0 (16%) but also contains a small proportion of very long-chain fatty acids (C22:0, 5%; C24:0, 2%; and C24:1, 1%). EPC was comprised of 16:0 (34%), 18:0 (11%), 18:1 (32%), 18:2 (18%) and 20:4 (3%).

2.2. Sample preparation

Samples for X-ray examination were prepared by mixing lipids in chloroform/methanol (9/1, vol/vol) in the indicated proportions. The solvent was subsequently evaporated under a stream of oxygen-free dry nitrogen at 45 °C and traces of residual solvent removed after a 2 day storage at 20 °C under high vacuum. Multilamellar vesicles (MLVs) were obtained after hydration (50 wt.%/wt.%) with an equal weight of buffer (10 mM Tris HCl, 150 mM NaCl, 0.1 mM CaCl₂). The dispersions were equilibrated under argon gas at 90 °C for 1 h with shaking (Eppendorf Thermomixer). The aqueous lipid dispersion was thoroughly stirred, sealed under argon and stored at 4 °C until thermal annealing prior to X-ray examination.

2.3. X-ray diffraction methods

X-ray scattering intensities measurements were performed on beamlines 6.2 and 16.1 of the Daresbury Synchrotron Radiation

Laboratory (Warrington, UK) following a protocol adapted from Tessier et al. [29]. The lipid dispersions (~15 µl) were warmed to 20 °C and stored for 3–6 h between two thin mica windows of the sample cell which was mounted on a programmable temperature stage (Linkam, UK). The temperature was monitored by a thermocouple (Quad Service, Poissy, France) inserted directly into the lipid dispersion. The initial thermal annealing by heating and subsequent cooling scans were performed at a rate of 20 °C/min over the temperature range 18 °C–90 °C–2 °C to ensure thorough mixing in the fluid phase. The scan in which the sample was exposed to the X-ray beam to record the scattering intensity patterns was performed at a rate of 2 °C/min from 2 °C to 46 °C. This thermal scan rate was selected to ensure minimal radiation damage to the sample while at the same time producing reversible thermotropic structural changes. Although complete equilibration may not be achieved the reversible changes observed in heating and subsequent cooling scans showed consistent effects of the presence of ceramide-rich structures. Small-angle X-ray scattering (SAXS) and wide-angle X-ray scattering (WAXS) intensity profiles were simultaneously recorded in 30 s time frames using an X-ray beam wavelength of 0.15 nm. The SAXS quadrant detector response was corrected for channel response using a static radioactive Fe source and S-calibrated (nm⁻¹) using hydrated rat tail collagen [30]. The WAXS intensity profiles were recorded using an INEL curved detector which was calibrated using high density polyethylene [31].

The small-angle X-ray scattering intensity profiles were analyzed using standard processing [32]. The scattering intensity data from four orders of Bragg reflections from the multilamellar liposomes were used to construct electron density profiles [33] for the single or for coexisting repeat structures detected in the lipid dispersions. After correction of the raw data for detector channel response and subtraction of the background scattering, each of the sets of small-angle peaks was deconvoluted by fitting a Lorentzian+Gaussian distribution to the scattering bands. The fits were performed with the Peakfit 4.12 (Systat Software Inc.) software. The square root of integrated peak intensity $I(h)$ was used to determine the form factor $F(h)$ of each of the respective reflections, $F(h) = h\sqrt{I(h)}$, where h = order of peak reflection, $I(h)$ = integrated intensity of each respective reflection. The relative electron density profile was calculated by the Fourier synthesis:

$$\rho(z) = \sum \pm F(h) \cos(2\pi h z/d)$$

where d -spacing = $d_{pp} + d_w$ (d_{pp} is the bilayer thickness measured as the distance between the peaks of highest electron density representing the phosphate groups of the phospholipids and d_w is the thickness of the hydration layer). Measurements were conducted at a resolution of $d/2h_{max} = 0.3$ nm for four orders.

The phase sign of each diffraction order is either positive or negative for a centrosymmetric electron density profile for lamellar gel, liquid-ordered and liquid-disordered phases. The phasing choice (---) was made because only this single combination of signs provides the expected electron density profile with the minimum density appropriately located at the bilayer center, the maxima at the 2 electron dense interfaces and the hydration layer density ($0.33e^{-}/\text{\AA}^3$) at the intermediate value on the relative electron density scale. All other possible phase combinations result in aberrant distributions. The choice of phase angles was consistent with alternative methods of determination for aqueous dispersions of choline phosphatides [34,35]. Although the electron density profile of the fully hydrated phases was not highly resolved (only four orders of reflection were used), the calculated profiles provide reliable estimates of the bilayer thickness and interbilayer distances.

2.4. ESR spectroscopy measurements

X-band ESR experiments have been carried out to extend the range of our observations to the nanometer scale and to determine the

influence of the different components in complex mixtures systems on the molecular ordering. For that purpose we have used a doxyl-stearic acid spin probe labeled in position 16 of the chain (denoted hereafter 16NS) which undergoes tumbling in the fast motional regime, providing a reasonable spectral resolution over the temperature range (22 °C to 57 °C).

Lipid mixtures were doped with 0.1 mol% of 16NS (Avanti Polar Lipids). After evaporation of the solvent the dry lipids were hydrated with a large excess 500 μ l of buffer consisting of 10 mM Tris-HCl, pH7.5, 150 mM NaCl, 0.1 mM CaCl₂. The lipid dispersion was centrifuged and 20 μ l of the pelleted liposomes was transferred to an ESR measurement capillary cell and sealed. Continuous wave-ESR spectra were recorded at 9.5 GHz (Bruker, ER 200D ESR, Wissembourg, France) after an equilibration time (ca. 10 min) at each temperature set by the variable temperature device (Bruker ER4111VT). The signal was digitized by the EPRWARE software (Scientific Software Service, Bloomington, IL61701, USA). The ESR parameters have been obtained from least-squares fittings of spectra utilizing methods reported elsewhere [36,37] (see also www.esr-spectsim-softw.fr). The analyses are performed on the explicit assumptions of a single site, two sites without exchange exemplified in Fig. 1 or two sites with intersite exchange and three sites without exchange as demonstrated in Fig. 2; details of the methods used in the analysis are presented in the Supplementary data.

For each site the adjustable parameters of the fit are: 1) the reorientation correlation time τ and the order parameter S_{zz} of the Z axis of the \mathbf{g} and of the hyperfine coupling \mathbf{A} tensors parallel to the direction joining carbons no. 15 and 17 of the chain; 2) the Lorentzian broadening ΔL due to electron spin-spin interactions, independent of rotational and segmental motions and 3) the Gaussian broadening ΔG corresponding to unresolved proton hyperfine splitting. For the two-site model applied to the EPC/ECER and EPC/ECER/CHOL systems, the additional parameters are the fraction of the probe in the most ordered site denoted hereafter site A and the exchange rate ν_{ex} between sites A and B. The choice between the one-site and two-site models is not only based on the least-squares difference σ between the experimental and fitted spectra but also on the consistency of the results e.g. for a given phase S_{zz} cannot increase increasing temperature. It happens indeed that in some cases good spectral fittings can be achieved with inconsistent parameters. In most cases however, it was found that in the binary and ternary mixtures the two-site model is the most likely with $\sigma=0.6-0.8$ against $\sigma=1.1-1.5$ for a single site. With the exception of pure EPC indeed, the single-site model fails to provide a correct fit to the high field line of the spectra

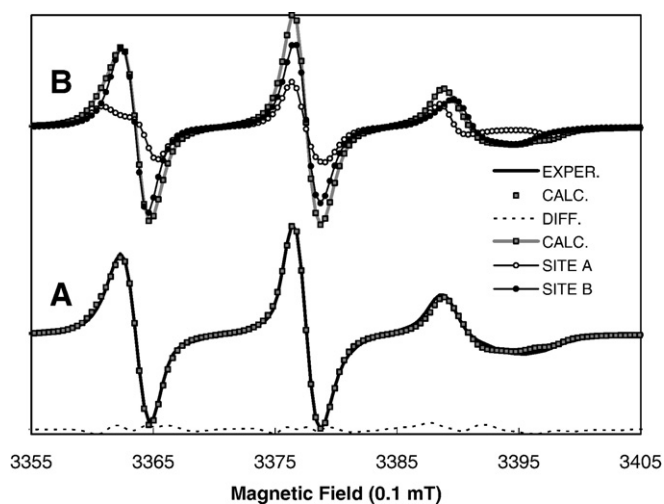


Fig. 1. (A) Experimental and computed spectra of the doxyl-16-stearic probe (16 NS) in EPC 70%, ECER 10%, CHOL 20% mixture at 37 °C. (B) Components of the spectrum computed with $S_{zz}=0.25$, $S_{zz}=0.12$ for site A and B, respectively. The fraction of site A is 33%.

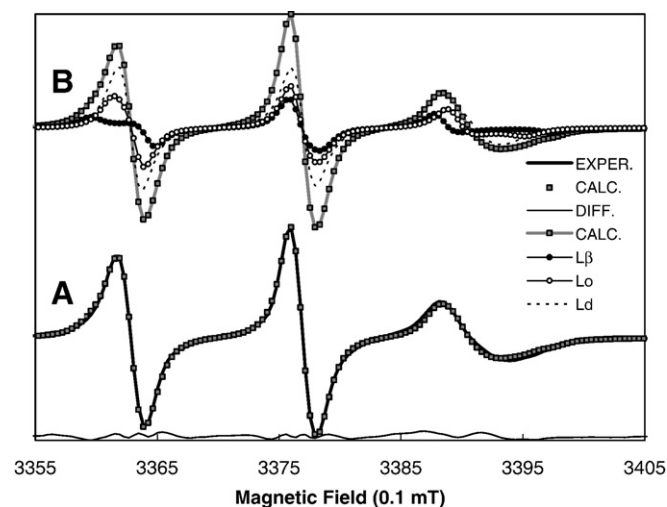


Fig. 2. (A) Experimental and computed spectra of the 16NS probe in the EPC 60%, ESM 20%, ECER 10%, and CHOL 10% mixture at 37 °C. (B) Components of the spectrum computed with $S_{zz}=0.27$, 0.15 and 0.07 for the L_{β} , L_o and L_d phases. The relevant fractions are 0.22, 0.28 and 0.48.

examined. The assumption of an intersite exchange does not improve the fittings and provides spurious values of ν_{ex} without coherent temperature dependence. This means that the exchange rate, if any, is in all cases examined here below the threshold of determination estimated to 10^6 s⁻¹.

The three-site model has only been found to be relevant to the quaternary system (EPC, ESM, ECER, and CHOL) where XRD experiments show also the coexistence of three phases (L_d , L_o and L_{β}). Owing to the number of parameters involved in spectral simulations, the intersites exchange has not been considered in this case.

Generally the coexistence of two or three sites is not revealed by visual inspection of the spectrum but by its least-squares fitting provided that the S_{zz} of its components differ by at least 20%. Although the partition coefficients of the ESR probe are unknown it is assumed that the integrated intensities of the spectral components are proportional to the fractions of the different sites or phases.

In the fast motional regime the reorientation correlation time of the probe is obtained from the dependence of the Lorentzian line widths denoted $\Delta B(M_i, \tau)$ upon the nitrogen nuclear magnetic quantum number $M_i=1, 0, -1$ and the reorientation correlation time τ . For a given value of τ , the $\Delta B(M_i, \tau)$ values decrease as S_{zz} increases and are intrinsically smaller in ordered sites than in disordered ones. As the residual dipolar electron spin-spin coupling ΔL increases with the molecular ordering [38] it is generally twice or more greater in L_{β} or L_o phases than in L_d phase. Spectral fittings reveal that when $\Delta L \gg \Delta B(M_i, \tau)$ the values of τ derived thereof are no longer reliable. The values of reorientation times are given for the L_d phase in Table 1 of the Supplementary data.

3. Results

3.1. Pure egg yolk phosphatidylcholine (EPC)

X-ray scattering intensity profiles of a control dispersion of EPC exhibit the characteristics of a liquid-disordered lamellar phase in the temperature range 2 °C–46 °C (data not shown). It is defined by broad peak observed in WAXS centered at d -spacing that 0.453 nm is characteristic of acyl chains in disordered liquid-crystalline structure (L_d). A lamellar arrangement was confirmed by even repeat distances between the multiple orders (SAXS). The L_d bilayer thickness as judged from the distance between the peaks of highest electron density in calculated electron density profiles through the lamellar d -spacing at a temperature of 22 °C and 38 °C is presented in Table 1. A

Table 1
Values of d -spacings and bilayer thickness for each of the identified phases derived after relative electron density calculations: $d(L_d)$, $d(L_o)$, $d(L_\beta)$ (d -spacing) and dL_d , dL_o , dL_β (bilayer thickness) of liquid-disordered, liquid-ordered and gel phase, respectively

| T | $d(L_d)$ [nm] | $d L_d$ [nm] | | | | | |
|-----------------------------------|---------------|--------------|----------------------------|---------------------------|-------------------|------------------|------------------|
| EPC | | | | | | | |
| 22 °C | 5.86 | 3.6 | | | | | |
| 38 °C | 5.75 | 3.5 | | | | | |
| T | $d(L_d)$ [nm] | $d L_d$ [nm] | $d(L_o)$ [nm] ^a | $d L_o$ [nm] ^a | $d(L_\beta)$ [nm] | $d L_\beta$ [nm] | $d L_\beta$ [nm] |
| EPC/ECER 90/10 | | | | | | | |
| 14 °C | 6.04 | 3.7 | 6.38 | 3.9 | 7.08 | 4.2 | |
| 22 °C | 5.95 | 3.7 | 6.35 | 3.9 | 7.07 | 4.2 | |
| 38 °C | 5.88 | 3.6 | 6.28 | 3.8 | 6.72 | 4.1 | |
| 46 °C | 5.79 | 3.6 | 6.03 | 3.7 | – | – | |
| EPC/ECER/CHOL 80/10/10 | | | | | | | |
| 14 °C | 6.29 | 3.8 | 6.49 | 4.0 | 7.01 | 4.2 | |
| 18 °C | 6.28 | 3.8 | 6.47 | 4.0 | 6.98 | 4.2 | |
| 22 °C | 6.21 | 3.8 | 6.43 | 3.9 | 6.96 | 4.3 | |
| 26 °C | 6.20 | 3.8 | 6.39 | 4.0 | 6.88 | 4.2 | |
| 30 °C | 6.14 | 3.7 | 6.31 | 3.9 | 6.71 | 4.0 | |
| 38 °C | 6.09 | 3.7 | 6.28 | 3.9 | 6.66 | 3.9 | |
| 46 °C | 6.06 | 3.7 | 6.21 | 3.8 | – | – | |
| EPC/ECER/CHOL 70/10/20 | | | | | | | |
| 14 °C | 6.31 | 3.8 | 6.53 | 4.0 | 6.76 | 4.3 | |
| 18 °C | 6.30 | 3.8 | 6.44 | 3.9 | 6.75 | 4.3 | |
| 22 °C | 6.21 | 3.8 | 6.41 | 3.9 | 6.62 | 4.1 | |
| 26 °C | 6.19 | 3.8 | 6.39 | 3.9 | 6.60 | 4.1 | |
| 38 °C | 6.08 | 3.8 | 6.32 | 3.9 | – | – | |
| 46 °C | 5.99 | 3.8 | 6.18 | 3.8 | – | – | |
| EPC/ECER/CHOL 60/10/30 | | | | | | | |
| 18 °C | 6.28 | 3.9 | 6.53 | 4.0 | 6.74 | 4.2 | |
| 22 °C | 6.20 | 3.8 | 6.53 | 4.1 | – | – | |
| 38 °C | 6.08 | 3.8 | 6.51 | 3.8 | – | – | |
| 46 °C | 5.99 | 3.7 | 6.35 | 3.8 | – | – | |
| EPC/ESM/ECER/CHOL 50/30/10/10 | | | | | | | |
| 22 °C | 6.43 | 4.3 | | | 6.69 | 4.6 | 4.7 |
| 38 °C | 6.28 | 4.2 | | | 6.69 | 4.6 | 4.7 |
| EPC/ESM/CHOL 65/17.5/17.5 | | | | | | | |
| 22 °C | 6.32 | 4.3 | | | 6.62 | 4.5 | – |
| 38 °C | 6.14 | 4.2 | | | 6.56 | 4.5 | – |
| EPC/ESM/ECER/CHOL 55/17.5/10/17.5 | | | | | | | |
| 22 °C | 6.38 | 4.4 | | | 6.64 | 4.5 | 6.96 |
| 38 °C | 6.20 | 4.3 | | | 6.55 | 4.5 | 6.77 |

^a This L_o phase can be distinguished from those formed in the presence of sphingomyelin as they are relatively more disordered on ESR criteria.

liquid-disordered phase arrangement is consistent with an inverse relationship between the lamellar d -spacing and temperature.

3.2. Binary mixtures of egg yolk phosphatidylcholine/ceramide (EPC/ECER)

To determine the effect of ECER on the thermotropic phase behavior and structure of EPC, codispersions of EPC with 10%, 20% and 30% ECER were examined.

3.2.1. EPC/ECER; 90/10

Two coexisting lamellar phases can be seen in the mixed aqueous dispersion over the entire temperature range of the scan from 2 °C to 46 °C (Fig. 3). A symmetrical sharp WAXS peak centered at 0.425 nm was observed up to a temperature of about 36 °C assigned to a gel phase with non-tilted hexagonally packed acyl chains (Fig. 3B).

A SAXS peak with a d -spacing of 7.07 nm at 22 °C is seen to undergo a decrease in lamellar d -spacing at temperatures coinciding with a decrease and eventual disappearance of the sharp WAXS peak.

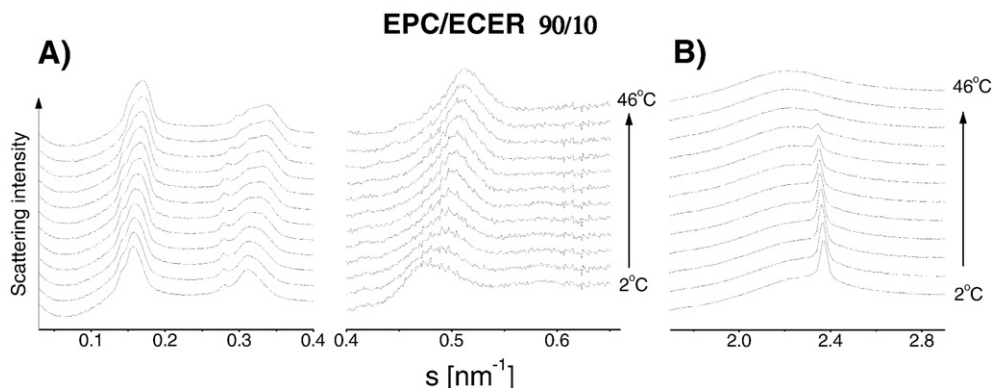


Fig. 3. Small-angle (A) and wide-angle (B) X-ray scattering intensity profiles recorded from a dispersion of a binary mixture of EPC/ECER (90/10) during a heating scan at 2 °C/min in the temperature range 2 °C–46 °C. (A) First- and second-order; (B) third- and fourth-order SAXS Bragg reflections; (C) WAXS region.

This SAXS peak is assigned as the lamellar gel phase. The other Bragg reflections are assigned on the basis of a broad scattering band in the WAXS region and the higher-order reflections in the SAXS region to the lamellar-disordered structures.

A detailed analysis of the scattering intensity peaks in the small-angle region was undertaken using peak fitting procedures to deconvolve parameters of the component lamellar structures. The results are presented in Fig. 4. This shows the first two orders of lamellar reflections that can be deconvoluted in three coexisting structures at temperatures of 22 °C (Fig. 4A) and 38 °C (Fig. 4B). Plots of the lamellar d -spacings and relative scattering intensities of the structures as a function of temperature are shown in Figs. 4C and 4D, respectively. The temperature dependence of the structure assigned as lamellar gel is seen to be independent of the two liquid-ordered lamellar structures which appear to be interconvertible with one another. The criteria for the assignment of the (two) liquid-disordered lamellar structures with smaller d -spacing are based on the disordered hydrocarbon chain configurations with WAXS intensities contributing to a broad band centered at a spacing of 0.451 nm. It is noteworthy that mixtures of dipalmitoylphosphatidylcholine containing about 10 mol% bovine brain ceramide exhibit multiple endothermic peaks at temperatures above T_m of the phospholipid which was interpreted as a preferential partition of ceramide in the liquid-crystal rather than the gel phase of the phospholipid [39].

The structures of the individual lamellar phases at designated temperatures were determined from calculated electron density profiles through the bilayer repeats. Values for bilayer thickness and interbilayer water distance together with lamellar d -spacing determined from 4 orders of reflection at 14 °C, 22 °C, 38 °C and 46 °C are collated in Table 1. It can be seen that bilayer thickness of the lamellar gel structure is constant between 14° and 22° but decreases with increasing temperature coinciding with disordering of the hydrocarbon chains. Bilayer thickness and interbilayer distance of the two lamellar-disordered structures both decrease progressively with increasing temperature but the rate of change of the interbilayer distance is greater for the disordered lamellar phase with the higher d -spacing. This indicates that the forces responsible for maintaining interbilayer space are different in the two structures inferring a difference in lipid composition.

3.2.2. EPC/ECER; 80/20

To confirm structural assignments an X-ray scattering examination of a mixed aqueous dispersion containing 20 mol% ECER was undertaken using the same experimental protocol. The results (not shown) were similar to the dispersion containing 10% ECER except that a gel phase in this binary mixture was observed in the whole temperature range 2 °C–46 °C. The SAXS intensity profiles also demonstrate gel/liquid-disordered phase coexistence for all four

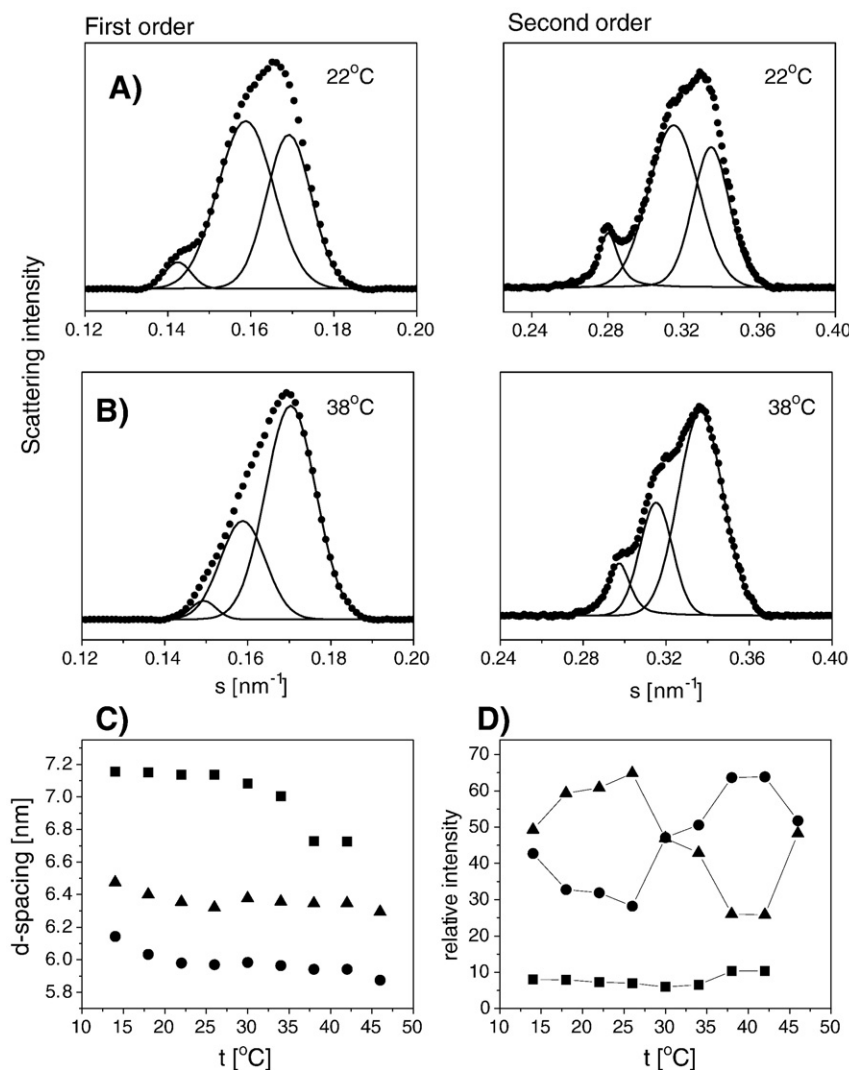


Fig. 4. Peak fit analysis of the first two orders of the Bragg scattering intensity peaks in the small-angle region. Deconvolution of three coexisting structures at 22 °C (Fig. 4A) and 38 °C (Fig. 4B). Plots of the lamellar d -spacings and relative scattering intensities of the structures as a function of temperature are shown in panels C and D, respectively.

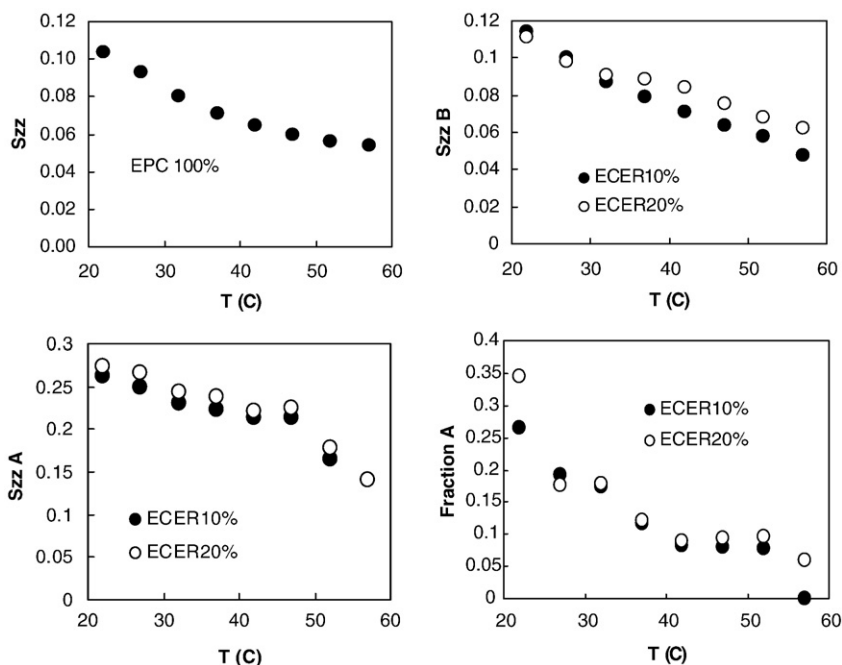


Fig. 5. Order parameters of 16NS and fraction of the ordered site, A, variation as a function of temperature in pure EPC and in EPC/ECER binary mixtures. ECER 10 and ECER 20: 10% and 20% ECER mole fraction.

orders of reflection. During the heating scan the d -spacing of the gel phase remained constant in contrast to the temperature dependence of the disordered lamellar phases.

Molecular order parameters and proportions of ordered and disordered structures in mixed EPC/ECER dispersions as a function of temperature were determined by ESR spectroscopy and results are presented in Fig. 5. The A and B sites observed by ESR may be ascribed to L_{β} and L_d phases evidenced by X-ray scattering data. The resolution, however, is probably not sufficient to distinguish the spectral components associated with the two lamellar-disordered phases in the EPC/ECER mixtures if the difference of the respective order parameters is too small. In site A, the order parameter is independent of the ECER concentration and shows only a small temperature dependence at high temperatures (Fig. 5), consistent with the invariant d -spacing of the gel phase. It may be pointed out that even in this phase, the 16NS probe shows a large reorientation freedom resulting in S_{zz} values less than 0.3. The onset of the melting of gel phase is shown by the steep variation of S_{zz} above 47 °C. In the L_d

phase, the influence of ECER on the molecular ordering is evidenced by the slight difference of S_{zz} values observed between 10 mol% and ECER 20 mol% fractions suggesting a partial intermixing of ECER and EPC.

3.3. Ternary mixtures of egg yolk phosphatidylcholine/ceramide/cholesterol (EPC/ECER/CHOL)

Dispersions containing 10% ECER and varying proportions of EPC and cholesterol were examined by X-ray and ESR spectroscopy to determine the effect of cholesterol on the phase behavior of ECER in a phospholipid bilayer. An overview of the thermotropic structural changes in a ternary mixture consisting of EPC/ECER/CHOL; 60/10/30 is presented in Fig. 6. This shows SAXS (Fig. 6A) and WAXS (Fig. 6B) intensity profiles at 4 °C intervals during a heating scan from 2 °C to 46 °C. It can be seen from four orders of lamellar repeat structures that there are coexisting bilayer phases throughout the temperature scans. A gel phase is present up to about 18 °C characterized by a sharp peak

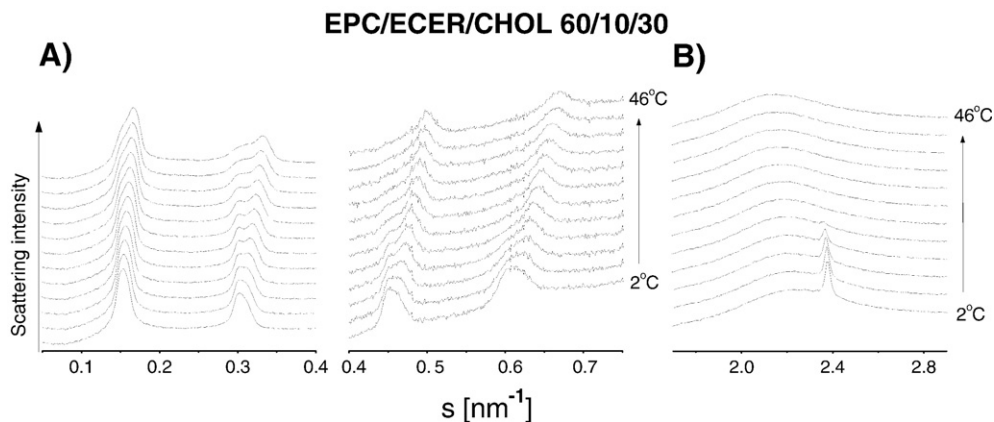


Fig. 6. Small- (A) and wide-angle (B) X-ray scattering intensity profiles of hydrated (50 wt.%/wt.%) ternary mixture EPC/ECER/CHOL (60/10/30; mol/mol) during a heating scan at 2 °C/min in the temperature range 2 °C–46 °C.

in the WAXS region centered at a d -spacing of 0.425 nm. Detailed analyses of the powder patterns recorded from this mixture and from heating scans of ternary mixtures containing 10 mol%, 20 mol% and 30 mol% cholesterol were undertaken.

3.3.1. EPC/ECER/CHOL; 80/10/10

Compared to the binary mixture EPC/ECER; 90/10 (Fig. 3C) the addition of cholesterol to the mixture in an equimolar amount to that of ECER does not alter the temperature of the gel-to-fluid transition detected in the WAXS region (data not shown). However, relatively broad asymmetrical peaks are observed for SAXS intensity reflections. These peaks were subject to analysis using Peakfit software and the result for the second-order peak is presented in Fig. 7B. A broadening of this peak is consistent with the coexistence of gel and liquid-disordered domains as delineated by peak deconvolution. A two and a three-phase coexistence model were tested to determine the most reliable interpretation based on both lamellar d -spacing and bilayer thickness. The latter parameters were derived from relative electron density calculations using the first four orders of reflection. The

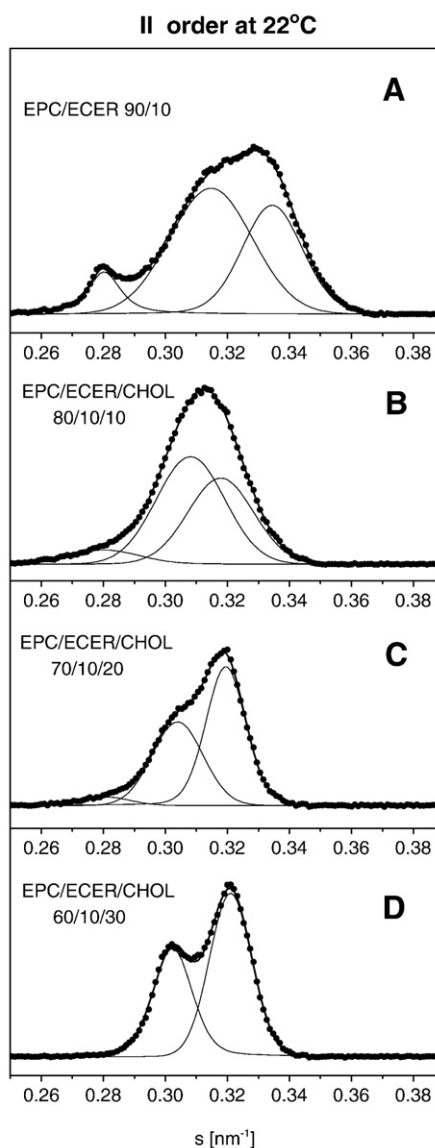


Fig. 7. Peak fit analyses of the SAXS second-order intensity peaks of the binary and ternary mixtures at 22 °C. All mixtures except EPC/ECER/CHOL (60/10/30) exhibit an L_{β}^s/L_d phase coexistence at this temperature. In the EPC/ECER/CHOL (60/10/30) mixture only an L_o/L_d liquid–liquid immiscibility is present above the L_{β} phase transition (18 °C).

d -spacing and bilayer thickness values obtained for the gel phase (6.41 nm, 3.9 nm at 22 °C) of the two-phase coexistence model were significantly less than expected when compared with observed values for the gel phase in the EPC/ECER 90/10 mixture (7.07 nm, 4.2 nm at 22 °C, Table 1). Furthermore, there was a temperature dependence of this d -spacing which is inconsistent with the characteristics of a gel phase. Alternatively, a fit to the Bragg peaks of a three-phase coexistence model provides a reliable interpretation of the scattering data with a relatively small peak centered at about 6.95 nm and a bilayer thickness of 4.2 nm which remains constant up to 26 °C and disappears at temperatures above 38 °C. This was tentatively assigned to a gel-to-fluid transition of the structure. The two larger peaks centered at 6.21 and 6.43 nm at 22 °C (Table 1) are assigned as lamellar fluid phases. The lamellar repeat spacing and bilayer thicknesses of these two structures decrease with increasing temperature over the entire heating range of 2 °C to 48 °C. These two lamellar structures have relatively disordered hydrocarbon chains as evidenced by a dominant broad scattering band in the WAXS region.

3.3.2. EPC/ECER/CHOL; 70/10/20 and EPC/ECER/CHOL; 60/10/30

In the presence of higher proportions of cholesterol there is a decrease of 8 °C in the gel-to-fluid transition in EPC/ECER/CHOL; 70/10/20 (data not shown) and a reduction of 16 °C in EPC/ECER/CHOL; 60/10/30 mixture (Fig. 6) compared to that recorded in a EPC/ECER; 90/10 binary mixture (Fig. 3). Thus gel–fluid coexistence evidenced from both SAXS and WAXS intensity profiles is observed in the temperature range 2 °C–26 °C (Fig. 4C) and 2 °C–18 °C (Fig. 6A), for the 70/10/20 and 60/10/30 ternary mixtures of EPC/ECER/CHOL, respectively. Liquid–Liquid immiscibility above the gel transition temperature, is consistent with both the asymmetric SAXS peaks of the mixture containing 20% cholesterol (temperature range 26 °C–42 °C) (data not shown) and two well resolved peaks for the mixture containing 30% cholesterol (18 °C–42 °C) (Fig. 6A). The number of distinct coexisting phases has also been examined in the SAXS reflections using peak fitting methods for scattering profiles recorded during the heating scans. With an analysis assuming a two-phase coexistence model, the results show that the presence of cholesterol increases d -spacing and bilayer thickness of the lamellar phase of smaller d -spacing. According to this model, gel d -spacings for the mixtures at 18 °C are 6.5 nm, (80/10/10); 6.6 nm, (70/10/20); 6.6 nm, (60/10/30) respectively. By contrast the bilayer thickness remains constant (4 ± 0.1 nm). Nevertheless the thickness values for bilayers in gel phase obtained with this model are less than those measured for gel phase in the binary mixture of EPC/ECER 90/10, (Table 1). The only plausible explanation for a decrease in bilayer thickness is that cholesterol is a component of the gel phase and this is not consistent with the well known effects of cholesterol in preventing molecular packing required for a creation of a gel phase.

An alternative analysis of the X-ray data from binary EPC/ECER; 90/10 mixtures and ternary mixtures containing cholesterol is to use a three-phase model (gel(L_{β})/intermediate liquid-disordered phase (L_o)/liquid-disordered phase(L_d)) with bilayer thickness in the order $L_{\beta} > L_o > L_d$. The intermediate arrangement may result from the reduction of the strong hydrophobic mismatch between L_{β} and L_d .

A three-phase rather than a two-phase coexistence model is assumed for ternary mixtures, as d -spacing values for gel phase are similar to that observed in the EPC/ECER; 90/10 mixture (Table 1). The mean gel bilayer thickness value is invariably in the range 4.2–4.3 nm in binary and ternary mixtures over temperatures ranging from 14 °C to the gel-phase transition temperature. This three-phase coexistence analysis identifies two liquid-disordered phases differing in lamellar repeat spacing by more than 0.1 nm. Above the transition temperature of the gel phase only L_i/L_d liquid–liquid immiscibility is observed (Fig. 7D).

The fittings of ESR spectra have been carried out under the assumptions of two or three coexisting sites. For the ternary mixtures, the two-site model assumption yields reliable results nearly indepen-

dent of starting parameters whereas the three-site model assumption gives spurious values of the order parameters and component fractions.

The peak characterizing the L_{β} phase in WAXS disappears above 38 °C, 26 °C and 18 °C for 10%, 20% and 30% CHOL mole fractions, respectively. However, above these temperatures, the A fraction does not decrease to zero and there are no obvious discontinuities in the S_{zz} vs. T plots (Fig. 8). This suggests that the site A corresponds successively to $L_{\beta}+L_o$ and L_o phases as the temperature is raised. In the domain of coexistence of these two phases, the difference in the values of S_{zz} is probably too small (<15%–20%) to separate the relevant spectral components. The correspondence between the L_1 phase identified by XRD and the A site evidenced by ESR explains why S_{zz} increases and becomes more temperature independent with increasing CHOL concentrations. Parallel to this, the fraction of this site shows a strong CHOL dependence as a function of temperature. At 30% CHOL, the fraction is quasi temperature independent up to 50 °C.

For site B, the less ordered component in ESR spectrum, there is a marked dependence of S_{zz} on the CHOL concentration (Fig. 8) which may be ascribed to the existence of short-lived complexes involving 2 or 3 molecules [40], e.g. EPC and CHOL, resulting in an increase of the average

molecular order probed by 16NS. The ordering effect of cholesterol is correlated with the increase of the bilayer thickness mentioned above for the L_o and L_d phases compared to the EPC/ECER mixtures.

The effect of ESM or ECER on the thermotropic structural changes in dispersions of quaternary mixtures of the four lipids was examined by X-ray diffraction in mixtures comprised of varying molar proportions of EPC/ESM or EPC/ECER.

3.4. Quaternary mixtures of egg yolk phosphatidylcholine/sphingomyelin/ceramide/cholesterol (EPC/ESM/ECER/CHOL; varying ESM)

The effect of addition of (up to 30 mol%) egg sphingomyelin to ternary mixtures EPC/ECER/CHOL was investigated. An overview of the thermotropic structural changes in the quaternary mixture consisting of EPC/ESM/ECER/CHOL; 50/30/10/10 is seen in Fig. 9. The first four orders of reflection of lamellar repeats (Fig. 9A) show coexistence of at least lamellar structures throughout the heating scan from 2 °C to 46 °C. These structures include both disordered and gel phase as evidenced by a sharp reflection superimposed on a broad

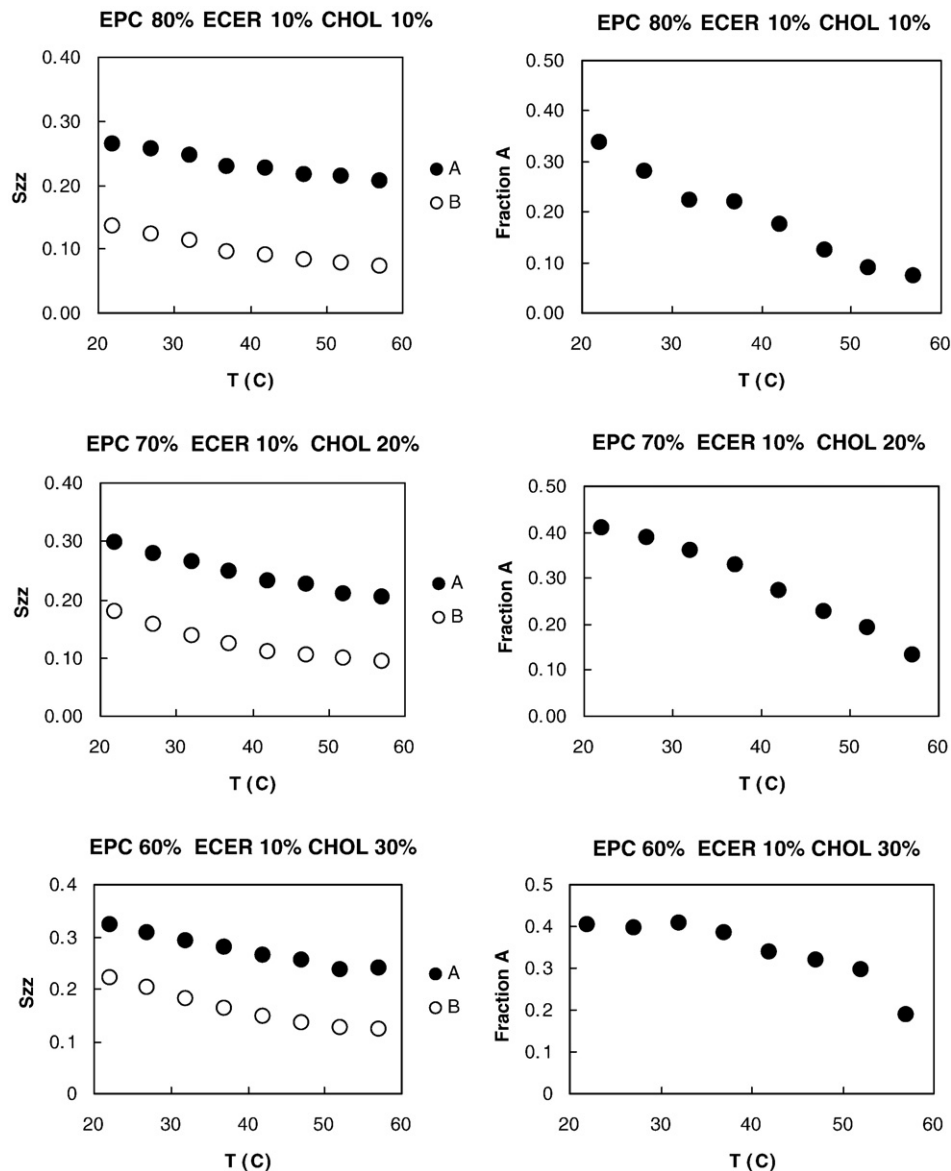


Fig. 8. Fraction of the ordered site A and temperature dependence of S_{zz} in sites A and B of ternary mixtures of EPC/ECER/CHOL spin-labeled with 16NS. Parameters are estimated by the fitting of ESR spectrum as indicated in Materials and methods.

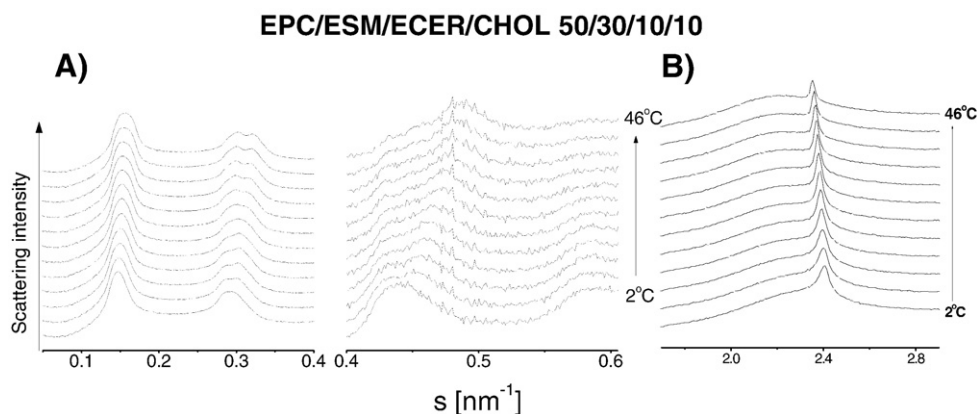


Fig. 9. Small-angle (A) and wide-angle (B) X-ray scattering intensity profiles recorded from an aqueous dispersion of a quaternary mixture of EPC/ESM/ECER/CHOL; (50/30/10/10) during heating scan of 2 °C/min in the temperature range 2 °C–46 °C.

scattering band in the WAXS region (Fig. 9B). A detailed analysis of this mixture and quaternary mixtures containing 5, 10 and 20 mol% ESM was undertaken.

3.4.1. EPC/ESM/ECER/CHOL; 75/5/10/10; EPC/ESM/ECER/CHOL; 70/10/10/10

Addition of only 5 mol% sphingomyelin (data not shown) compared to the ternary EPC/ECER/CHOL; 80/10/10 mixture was sufficient to induce appearance of a gel phase above 38 °C supporting the gel–fluid phase coexistence in the quaternary mixtures at physiological temperatures. The gel state may be tentatively ascribed to ceramide enriched domains and/or ceramide sphingomyelin complexes with a melting temperature higher than pure egg sphingomyelin (42 °C) [22]. Similar findings were observed in the quaternary mixture containing 10 mol% ESM (data not shown).

3.4.2. EPC/ESM/ECER/CHOL; 60/20/10/10 and EPC/ESM/ECER/CHOL; 50/30/10/10

Addition of 20 and 30 mol% sphingomyelin allows identification of several coexisting lamellar arrangements above 22 °C. The SAXS/WAXS intensity profiles of a mixed aqueous dispersion of EPC/ESM/ECER/CHOL, containing 30% ESM (Fig. 9) indicate that at least one lamellar structure is in a gel configuration evidenced by the sharp peak in the WAXS region at temperatures up to at least 46 °C. The coexisting lamellar structures are tentatively assigned to gel(L_β),

liquid-ordered (L_o), and liquid-disordered (L_d) phase and the d -spacings of the respective structures are presented in Table 1. Peak deconvolution of the four orders of the Bragg diffraction seen in the SAXS region, using a three-phase model (L_β , L_o , L_d) is shown for EPC/ESM/ECER/CHOL; 50/30/10/10 mixture in Fig. 10. Electron density profiles of this quaternary mixture were calculated at temperatures of 22 °C and 38 °C. The derived d -spacings and bilayer thickness of each lamellar structure are also presented in Table 1. In contrast to the structure assigned as L_d , the bilayer thickness of L_o structure (4.6 nm) remained independent of temperature over this range (Table 1). With increasing temperature, a progressive transition of L_β into L_o is observed in Fig. 9A.

The order parameter, S_{zz} , of the spin probe and its distribution among the phases have been measured at variable ESM and ECER concentrations as a function of temperature and the results are presented in Fig. 11. In the quaternary mixtures containing the lowest proportion of ESM (10%) the fraction of the L_β phase, evidenced by the WAXS intensity, decreases linearly with increasing temperatures and coexists with the L_d phase in the whole temperature range examined. For the quaternary mixture containing 20% and 30% ESM, both X-ray diffraction and ESR spectroscopy indicate the coexistence of three phases L_β , L_o and L_d . The order parameters of the L_o phase are intermediate between the order parameters of the L_β and L_d phases. However, the L_o phase disappears above 42 °C for a mixture containing 20% ESM with a sharp increase of the L_d fraction. In the case of 30%

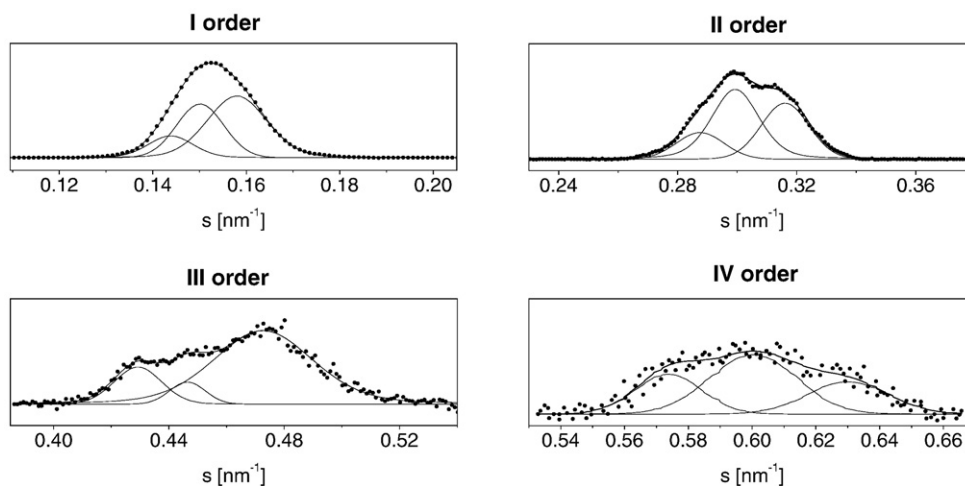


Fig. 10. Peak fit analysis of the SAXS intensity peaks. Deconvolution of three components is shown for the four orders from the EPC/ESM/ECER/CHOL; (50/30/10/10) quaternary mixture at 30 °C.

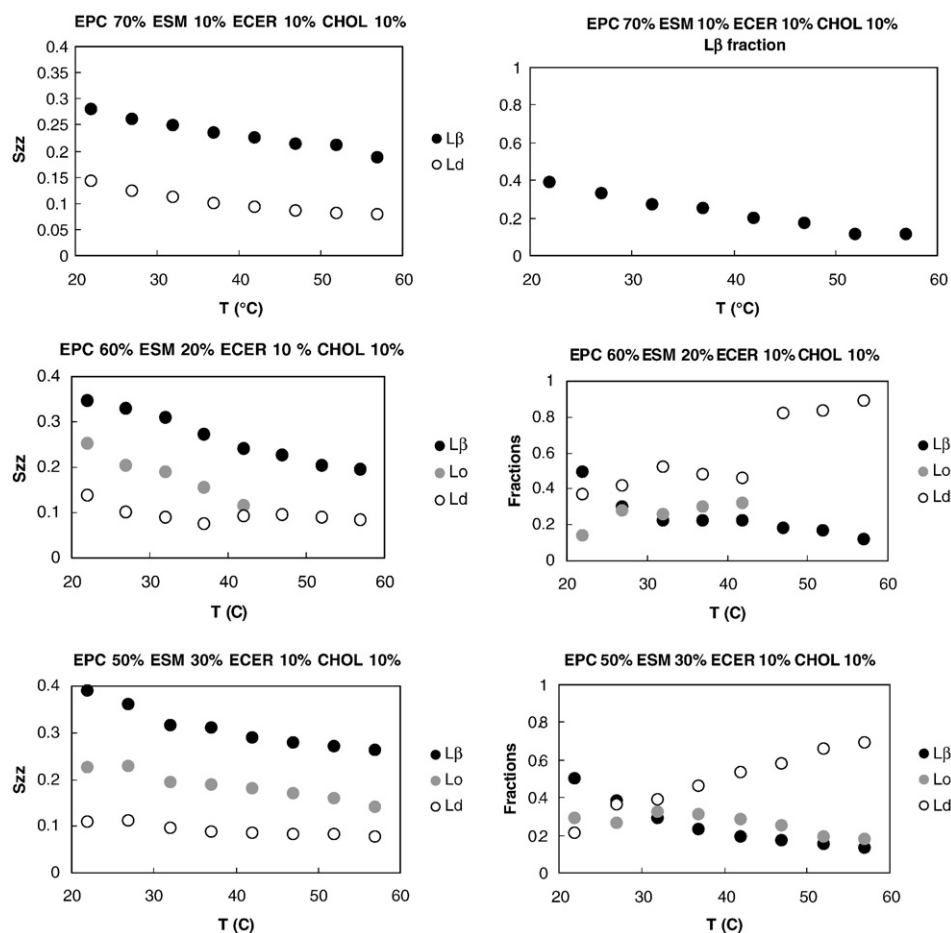


Fig. 11. Effects of the sphingomyelin concentration (10, 20, 30 mol%) on the fractions and order parameters of the L_β , L_0 and L_d phases in the EPC/ESM/ECER/CHOL mixtures.

ESM, there is a progressive decrease of the L_β and L_0 fractions at temperatures above 32 °C with a quasi-linear increase of the L_d fraction up to 57 °C.

3.5. Quaternary mixtures of egg yolk phosphatidylcholine/sphingomyelin/ceramide/cholesterol (EPC/ESM/ECER/CHOL; varying ECER)

Addition of only 5% of ECER to the mixture comprised of control EPC/ESM/CHOL; 65/17.5/17.5 is associated with the appearance of the L_β phase in the entire temperature range and this can be seen in a summary of the results presented in Fig. 12B. This contrasts with the behavior of the ternary mixture in the absence of ECER in which coexistence of only the L_0/L_d phases is observed between 2 °C and 42 °C (Fig. 12A). For the three quaternary mixtures progressively enriched in ECER (5, (Fig. 12), 10, 15 and 20 mol% (data not shown)), two coexisting lamellar structures are seen in the SAXS region, the larger d -spacing of which is assigned to a gel phase while the other is ascribed to a liquid phase. To obtain a more accurate understanding of the lipid phase structure a peak deconvolution analysis of the second-order Bragg peak was undertaken using initially a two-phase coexistence model and subsequently a three-phase coexistence model. The fits of the three-phase coexistence model lead to consistent estimates of bilayer thicknesses of about 4.4 nm, 4.5 nm and 4.7 nm for L_d , L_0 and L_β phase respectively at 22 °C (Table 1).

The packing density of the acyl chains of mixed aqueous dispersions was determined from WAXS d -spacings recorded during heating scans from 2 °C to 46 °C. The effect of increasing ESM in quaternary mixtures containing EPC/ECER/CHOL and of increasing ECER in quaternary mixtures containing EPC/ESM/CHOL on WAXS d -

spacing as a function of temperature is shown in Figs. 13A and 13B, respectively. These WAXS data show that increasing proportions of ESM in quaternary mixtures cause an increased packing density of the hydrocarbon region of the bilayers. A similar but more pronounced trend is observed with mixtures containing increasing proportions of ECER.

Additional studies of these mixtures were performed using spin-label methods to obtain information on the acyl chain ordering in the gel and fluid arrangements detected by X-ray scattering methods. Control ESR experiments show that in the EPC/ESM/CHOL mixture, only the L_0 and L_d phases coexist. It may be concluded that the existence of the L_β phase in the quaternary mixture is therefore due to the presence of ECER. Increasing the proportion of ECER in the mixture while keeping the proportions of ESM and CHOL constant results in an increase in S_{zz} in the L_β and L_d phases without marked effect on the L_0 phase (Table 2). The major effect is the reduction of the L_d fraction and the augmentation of S_{zz} in this phase. This is consistent with other studies showing that ECER, like CHOL form complexes with phospholipids and enhances the ordering of the hydrocarbon chains.

4. Discussion

The present results demonstrate that aqueous dispersions of relatively simple mixtures of lipids of biological origin exhibit highly complex thermotropic phase structure. This behavior often differs markedly from mixtures of chemically defined molecular species of the same lipid classes and emphasises the limitations of such model membranes to mimic the properties of biological membranes. By the same token, it is only by defining the properties of lipid assemblies

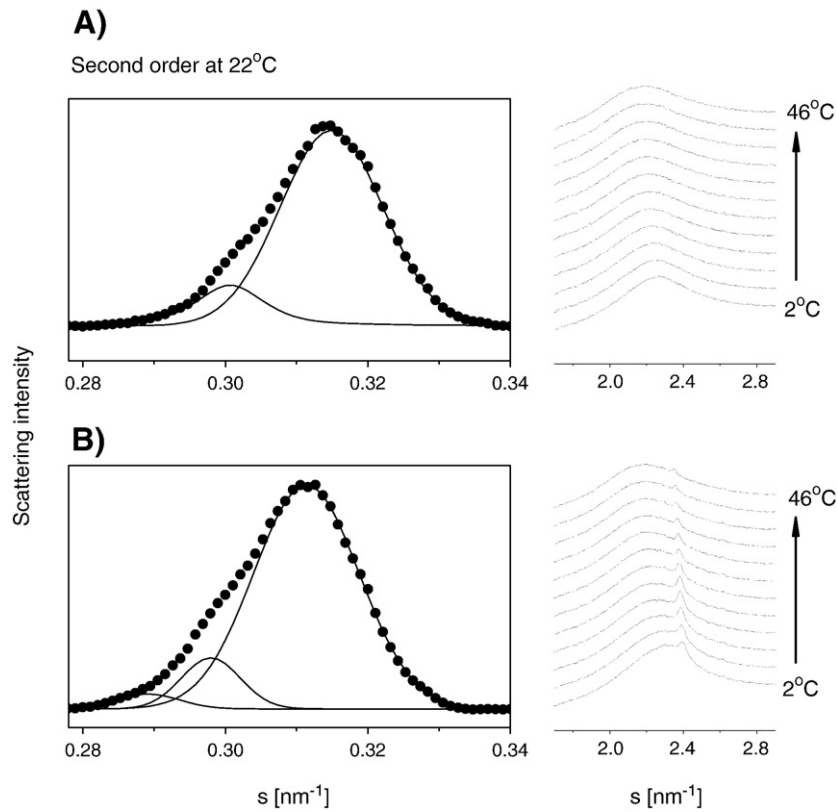


Fig. 12. Small-angle (second-order at 22 °C) and wide-angle X-ray scattering intensity profiles (2 °–46 °C) recorded from, (A) a ternary mixture of EPC/ESM/CHOL; 55/17.5/17.5 in which two liquid structures are resolved (L_o/L_d); (B) a quaternary mixture of EPC/ESM/ECER/CHOL; 55/17.5/5/17.5 in which a gel (L_{β}) and two liquid structures (L_o and L_d) are resolved.

comprised of the myriad of chemically defined molecular species found in cell membranes that an understanding of the dynamic structure of the lipid bilayer can be achieved.

We have used X-ray diffraction to provide information on the structure of lamellar phases formed by complex lipid mixtures. While scattering methods can give accurate estimates of bilayer repeat distances in multilamellar dispersions the method is unable to define the size of coexisting domains. Nevertheless, peak fitting procedures applied to powder diffraction patterns have been used to determine the relative proportions of coexisting structures by assuming that their respective form factors remain constant over a small range of scattering angles. Based on this curve fitting approach calculations of

electron density using four or so orders of reflection from SAXS intensity profiles have been performed and estimates of lipid and water thickness obtained with reasonable resolution. Parallel studies using ESR probe methods in which the dynamic motion of the probe is analyzed by spectral simulations to extract order parameters and reorientation correlation times have been used to complement the diffraction studies. The spectral analysis also provides an estimate of the proportion of probe partitioning between relatively ordered and disordered domains.

The richness of the phase properties of these complex molecular mixtures is exemplified by mixtures of phosphatidylcholine and ceramide. Aqueous dispersions of binary mixtures of palmitoyllecithin

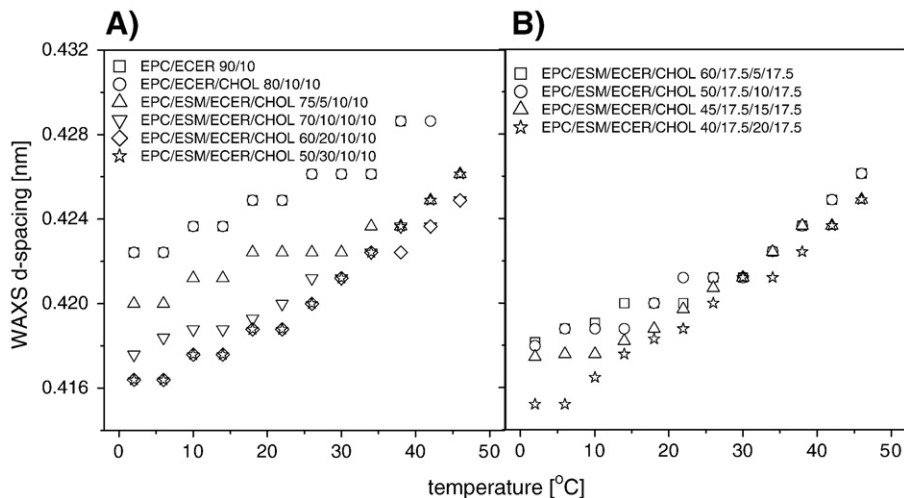


Fig. 13. WAXS d -spacings as a function of temperature for two series of quaternary mixtures indicated.

Table 2

Order parameters and partition coefficients of the spin-probe in the EPC/ESM/ECER/CHOL mixtures for different ECER concentrations

| I | EPC 65% | ESM 17.5% | CHOL 17.5% | | | |
|-------------------------------------|---------|-----------|------------|------------|------|------|
| II | EPC 60% | ESM 17.5% | ECER 5% | CHOL 17.5% | | |
| III | EPC 55% | ESM 17.5% | ECER 10% | CHOL 17.5% | | |
| IV | EPC 50% | ESM 17.5% | ECER 15% | CHOL 17.5% | | |
| V | EPC 45% | ESM 17.5% | ECER 20% | CHOL 17.5% | | |
| VI | EPC 35% | ESM 17.5% | ECER 30% | CHOL 17.5% | | |
| <i>T</i> | II | III | IV | V | VI | |
| <i>S_{zz} L_β</i> | | | | | | |
| 27 °C | 0.32 | 0.34 | 0.38 | 0.39 | 0.44 | |
| 37 °C | 0.29 | 0.28 | 0.32 | 0.35 | 0.39 | |
| 47 °C | 0.26 | 0.26 | 0.28 | 0.30 | 0.33 | |
| <i>S_{zz} L_o</i> | | | | | | |
| 27 °C | 0.29 | 0.21 | 0.22 | 0.24 | 0.25 | 0.29 |
| 37 °C | 0.26 | 0.18 | 0.19 | 0.21 | 0.23 | 0.26 |
| 47 °C | 0.25 | 0.15 | 0.16 | 0.19 | 0.19 | 0.22 |
| <i>S_{zz} L_d</i> | | | | | | |
| 27 °C | 0.11 | 0.10 | 0.13 | 0.13 | 0.12 | 0.16 |
| 37 °C | 0.07 | 0.09 | 0.09 | 0.09 | 0.12 | 0.14 |
| 47 °C | 0.07 | 0.08 | 0.09 | 0.09 | 0.10 | 0.12 |
| Fraction <i>L_β</i> | | | | | | |
| 27 °C | 0.30 | 0.30 | 0.36 | 0.39 | 0.50 | |
| 37 °C | 0.21 | 0.29 | 0.24 | 0.33 | 0.36 | |
| 47 °C | 0.17 | 0.21 | 0.22 | 0.23 | 0.27 | |
| Fraction <i>L_o</i> | | | | | | |
| 27 °C | 0.38 | 0.41 | 0.40 | 0.43 | 0.46 | 0.39 |
| 37 °C | 0.33 | 0.31 | 0.33 | 0.47 | 0.37 | 0.45 |
| 47 °C | 0.25 | 0.25 | 0.32 | 0.34 | 0.34 | 0.44 |
| Fraction <i>L_d</i> | | | | | | |
| 27 °C | 0.62 | 0.29 | 0.30 | 0.21 | 0.15 | 0.11 |
| 37 °C | 0.67 | 0.48 | 0.38 | 0.29 | 0.30 | 0.19 |
| 47 °C | 0.75 | 0.58 | 0.47 | 0.44 | 0.43 | 0.29 |

sphatidylcholine and ceramide exhibit gel–fluid phase coexistence over a wide composition range of the phase diagram but no evidence of liquid–liquid phase separation could be detected by ²H-NMR [41] or fluorescence probe methods [42,43]. The X-ray scattering and ESR spectroscopic data identify not only a relatively small (<10%) gel phase signature in the dispersion composed of EPC/ECER but also that the dominant phases are coexistence of two lamellar structures, one more ordered than the other. Upon heating from about 20 °C to 40 °C the more ordered of the two phases is progressively transformed into the more disordered structure. It is clear from this dispersion, and the dispersion comprised of 20 mol% ECER, that not all the ceramide forms gel phase and that some ceramide, possibly the less saturated molecular species [44] interacts with phosphatidylcholine to create a less disordered lamellar structure. The failure to detect liquid–liquid phase separations appears to be partly due to the methods used to examine the phase behavior of the pure lipid mixtures and to the differences between ternary mixtures of molecularly defined lipids and that of the very complex mixtures characterized by a wide range of molecular species. Thus the phase separation of a few molecular combinations among many molecular species may occur whereas with synthetic ternary mixtures there are only five possible combinations excluding cholesterol crystals.

It has been suggested that gel–fluid immiscibility in phospholipid–ceramide mixtures is driven by a mismatch in the length and extent of unsaturation of the hydrocarbon chains of the respective lipids [45,46]. This explanation can be excluded in the present mixtures because in the case of EPC/ECER containing 10 mol% ceramide only 1/100 chains is more than 18 carbons in length and a difference of at least four methylene groups is required to produce phase demixing [47]. The most likely explanation for the formation of gel structure is the strong intermolecular interactions between ceramide molecules forming a compact structure.

In the composition region of the ternary phase diagram of PC/CER/CHOL examined in the present study the most conspicuous effect of

cholesterol is to destabilize the gel phase formed by ceramide and to delineate more clearly the two fluid lamellar phases. This is evidenced by the marked decrease in gel-to-fluid phase transition of the ceramide-rich structure. Further evidence of the influence of cholesterol is the increase in thickness of the bilayer compared with dispersions of EPC and ECER in binary mixtures and the increased order of the hydrocarbon chains in fluid bilayers. This is consistent with studies of similar ternary mixtures which indicate that gel phase coexists with fluid-ordered-like phases [43]. On the basis of the order parameter data it is possible to designate these two lamellar phases as liquid-ordered and liquid-disordered, respectively. A comparison of order parameters derived from dispersions of EPC/ECER in the absence and presence of cholesterol is consistent with recent molecular dynamics simulations suggesting similar effects of ceramide and cholesterol on POPC bilayers but cholesterol has a much greater ability to order the acyl chains of the phospholipid than ceramide [48]. In the ternary mixtures we have examined neither the proportions of ceramide or cholesterol approach the solubility limits but clearly the tendency of ceramide to phase separate into a lamellar gel is counteracted by cholesterol despite the apparent preference of ceramide rather than cholesterol to interact with the phospholipid [23].

Studies of the quaternary mixtures containing sphingomyelins serve to highlight the competing affinities for association between the different lipid classes. Since the only component in the mixture capable of forming gel phase at temperatures greater than 45 °C is ceramide it is reasonable to assume that this lipid is enriched in gel structure. The gel phase, however, is stable at temperatures higher than ceramide alone in phosphatidylcholine bilayers when sphingomyelin is also present. This indicates that sphingomyelin may also be a component of the gel phase. Analysis of the WAXS data shows that in quaternary mixtures sphingomyelin not only stabilizes the gel phase but the packing density of the chains also increases. This increased chain density is reflected in the greater order parameter derived from the spin label studies. The formation of complexes between ceramide and sphingomyelin is supported by the report that bovine brain sphingomyelin forms a gel-phase complex with ceramide from the same source [22]. The coexistence of this gel phase with liquid-ordered phase implies that sphingomyelin also interacts with cholesterol thereby preventing cholesterol from destabilizing the ceramide-enriched gel phase. The preferential interaction of cholesterol with sphingomyelin is assumed because it is known that cholesterol has a much greater affinity for sphingomyelin than egg phosphatidylcholine [49,50]. Sphingomyelin appears to act in a dynamic manner in mediating transition between gel structure dominated by ceramide and liquid-ordered structure formed from interaction between sphingomyelin and cholesterol. This can be seen by the progressive replacement of gel structure with liquid-ordered structure with increasing temperature presumably as sphingomyelin is mobilized from the ceramide-rich gel phase.

The coexisting phase structures in these complex mixtures have implications for signaling pathways operating in the plasma membrane of living cells. Our earlier studies showed that ceramide enhances hydrolytic activity of phospholipase A2 in mixed substrate dispersions [8]. Furthermore, pretreatment of phosphatidylcholine/sphingomyelin liposomes with sphingomyelinase leads to increased phospholipase activity [51]. The action of sphingomyelinase on activating phospholipase has also been demonstrated at the cellular level with CHO-2B cells [51]. On the other hand, sphingomyelin in mixtures of phosphatidylcholine or phosphatidylethanolamine/phosphatidylserine inhibits phospholipase activity which, in turn, is counteracted by the presence of cholesterol [52]. Thus in terms of generation of lipid signals, sphingomyelinase action triggers phospholipase activity in three ways: 1. by the creation of ceramide-rich gel domains so-called “membrane heterogeneities” and the attendant formation of defects in the boundary regions; 2. by reduction in available sphingomyelin by interaction with ceramide-rich domains;

3. by formation of liquid-ordered phase as the proportion of cholesterol to sphingomyelin increases. Biochemical homeostasis to restore the resting phase state of the membrane could be by hydrolysis of ceramide or accumulation of lysophospholipid products and replenishment of sphingomyelin.

Acknowledgements

The work was aided by a grant from the Human Frontier Science Programme (RGP0016/2005C) and Bulgarian Ministry of Education and Science, National Programme for Development of Scientific Potential. G. Staneva is grateful to C. Tessier and P. Nuss for the many enlightening discussions.

Appendix A. Supplementary data

Supplementary data associated with this article can be found, in the online version, at doi:10.1016/j.bbmem.2008.07.025.

References

- [1] D.A. Brown, E. London, Structure and function of sphingolipid- and cholesterol-rich membrane rafts, *J. Biol. Chem.* 275 (2000) 17221–17224.
- [2] K. Simons, E. Ikonen, Functional rafts in cell membranes, *Nature* 387 (1997) 569–572.
- [3] K. Simons, E. Ikonen, Cell biology—how cells handle cholesterol, *Science* 290 (2000) 1721–1726.
- [4] Y.A. Hannun, Functions of ceramide in coordinating cellular responses to stress, *Science* 274 (1996) 1855–1859.
- [5] S. Manes, A. Viola, Lipid rafts in lymphocyte activation and migration (Review), *Molec. Membr. Biol.* 23 (2006) 59–69.
- [6] J.F. Hancock, Lipid rafts: contentious only from simplistic standpoints, *Nat. Rev. Molec. Cell Biol.* 7 (2006) 456–462.
- [7] A. Morales, H. Lee, F.M. Goni, R. Kolesnick, J.C. Fernandez-Checa, Sphingolipids and cell death, *Apoptosis* 12 (2007) 923–939.
- [8] K.S. Koumanov, A.B. Momchilova, P.J. Quinn, C. Wolf, Ceramides increase the activity of the secretory phospholipase A(2) and alter its fatty acid specificity, *Biochem. J.* 363 (2002) 45–51.
- [9] L. Scheffer, A.H. Futerman, L. Addadi, Antibody labeling of cholesterol/ceramide ordered domains in cell membranes, *Chembiochem.* 8 (2007) 2286–2294.
- [10] I. Johnston, L.J. Johnston, Sphingomyelinase generation of ceramide promotes clustering of nanoscale domains in supported bilayer membranes, *Biochim. Biophys. Acta* 1778 (2008) 185–197.
- [11] E.L. Laviad, L. Albee, I. Pankova-Kholmyansky, S. Epstein, H. Park, A.H. Merrill, A.H. Futerman, Characterization of ceramide synthase 2—tissue distribution, substrate specificity, and inhibition by sphingosine 1-phosphate, *J. Biol. Chem.* 283 (2008) 5677–5684.
- [12] T. Levade, J.P. Jaffrezou, Signalling sphingomyelinases: which, where, how and why? *Biochim. Biophys. Acta* 1438 (1999) 1–17.
- [13] R.J. Veldman, N. Maestre, O.M. Aduib, J.A. Medin, R. Salvayre, T. Levade, A neutral sphingomyelinase resides in sphingolipid-enriched microdomains and is inhibited by the caveolin-scaffolding domain: potential implications in tumour necrosis factor signalling, *Biochem. J.* 355 (2001) 859–868.
- [14] P.S. Liu, R.G.W. Anderson, Compartmentalized production of ceramide at the cell surface, *J. Biol. Chem.* 270 (1995) 27179–27185.
- [15] A. Cremesti, F. Paris, H. Grassme, N. Holler, J. Tschopp, Z. Fuks, E. Gulbins, R. Kolesnick, Ceramide enables Fas to cap and kill, *J. Biol. Chem.* 276 (2001) 23954–23961.
- [16] M.P. Veiga, J.L.R. Arrondo, F.M. Goni, A. Alonso, Ceramides in phospholipid membranes: effects on bilayer stability and transition to nonlamellar phases, *Biophys. J.* 76 (1999) 342–350.
- [17] R.N. Kolesnick, F.M. Goni, A. Alonso, Compartmentalization of ceramide signaling: physical foundations and biological effects, *J. Cell. Physiol.* 184 (2000) 285–300.
- [18] S. Hartel, M.L. Fanani, B. Maggio, Shape transitions and lattice structuring of ceramide-enriched domains generated by sphingomyelinase in lipid monolayers, *Biophys. J.* 88 (2005) 287–304.
- [19] J.M. Holopainen, M.I. Angelova, P.K.J. Kinnunen, Vectorial budding of asymmetric enzymic formation of ceramide in giant unilamellar vesicles, *Biophys. J.* 78 (2000) 830–838.
- [20] K. Trajkovic, C. Hsu, S. Chiantia, L. Rajendran, D. Wenzel, F. Wieland, P. Schwille, B. Brugger, M. Simons, Ceramide triggers budding of exosome vesicles into multivesicular endosomes, *Science* 319 (2008) 1244–1247.
- [21] J. Shah, J.M. Atienza, R.I. Duclos, A.V. Rawlings, Z.X. Dong, G.G. Shipley, Structural and thermotropic properties of synthetic C16-0 (palmitoyl) ceramide—effect of hydration, *J. Lipid Res.* 36 (1995) 1936–1944.
- [22] J.B. Massey, Interaction of ceramides with phosphatidylcholine, sphingomyelin and sphingomyelin/cholesterol bilayers, *Biochim. Biophys. Acta* 1510 (2001) 167–184.
- [23] P.S. Megha, E. London, Ceramide selectively displaces cholesterol from ordered lipid domains (rafts). Implications for lipid raft structure and function, *J. Biol. Chem.* 279 (2004) 9997–10004.
- [24] K.C. Tu, M.L. Klein, D.J. Tobias, Constant-Pressure molecular dynamics investigation of cholesterol effects in a dipalmitoylphosphatidylcholine bilayer, *Biophys. J.* 75 (1998) 2147–2156.
- [25] M. Pasenkiewicz-Gierula, T. Rog, K. Kitamura, A. Kusumi, Cholesterol effects on the phosphatidylcholine bilayer polar region: a molecular simulation study, *Biophys. J.* 78 (2000) 1376–1389.
- [26] P. Haberkant, O. Schmitt, F.X. Contreras, C. Thiele, K. Hanada, H. Sprong, C. Reinhard, F.T. Wieland, B. Brugger, Protein–Sphingolipid interactions within cellular membranes, *J. Lipid Res.* 49 (2008) 251–262.
- [27] Y. Taniguchi, T. Ohba, H. Miyata, K. Ohki, Rapid phase change of lipid microdomains in giant vesicles induced by conversion of sphingomyelin to ceramide, *Biochim. Biophys. Acta* 1758 (2006) 145–153.
- [28] I. Lopez-Montero, M. Velez, P.F. Devaux, Surface tension induced by sphingomyelin to ceramide conversion in lipid membranes, *Biochim. Biophys. Acta* 1768 (2007) 553–561.
- [29] C. Tessier, P. Quinn, K. Koumanov, G. Trugnan, D. Rainteau, C. Wolf, Modulation of the phase heterogeneity of aminoglycerophospholipid mixtures by sphingomyelin and monovalent cations: maintenance of the lamellar arrangement in the biological membranes, *Eur. Biophys. J.* 33 (2004) 513–521.
- [30] R.D.B. Fraser, T.P. Macrae, Unit-cell and molecular connectivity in tendon collagen, *Int. J. Biol. Macrol.* 3 (1981) 193–200.
- [31] E.J. Addink, J. Beintema, Polymorphism of crystalline polypropylene, *Polymer* 2 (1961) 185–193.
- [32] R.T. Zhang, R.M. Suter, J.F. Nagle, Theory of the structure factor of lipid bilayers, *Phys. Rev. E* 50 (1994) 5047–5060.
- [33] T.J. McIntosh, Effect of cholesterol on structure of phosphatidylcholine bilayers, *Biochim. Biophys. Acta* 513 (1978) 43–58.
- [34] C.R. Worthing, G.I. King, T.J. McIntosh, Direct structure determination of multilayered membrane-type systems which contain fluid layers, *Biophys. J.* 13 (1973) 480–494.
- [35] Z.W. Yu, P.J. Quinn, Phase-stability of phosphatidylcholines in dimethylsulfoxide solutions, *Biophys. J.* 69 (1995) 1456–1463.
- [36] C. Chachaty, E.J. Soulie, Determination of electron spin resonance static and dynamic parameters by automated fitting of the spectra, *J. Phys. III* 5 (1995) 1927–1952.
- [37] C. Wolf, C. Chachaty, Compared effects of cholesterol and 7-dehydrocholesterol on sphingomyelin–glycerophospholipid bilayers studied by ESR, *Biophys. Chem.* 84 (2000) 269–279.
- [38] M. Deschamps, I.D. Campbell, J. Boyd, Residual dipolar couplings and some specific motions for motional averaging, *J. Magn. Res.* 172 (2005) 118–132.
- [39] D.C. Carre, B. Maggio, Phase behaviour and molecular interactions in mixtures of ceramide with dipalmitoylphosphatidylcholine, *J. Lipid Res.* 40 (1999) 1978–1989.
- [40] A. Radhakrishnan, H. McConnell, Composition fluctuations, chemical exchange, and nuclear relaxation in membranes containing cholesterol, *J. Chem. Phys.* 126 (2007).
- [41] Y.W. Hsueh, R. Giles, N. Kitson, J. Thewalt, The effect of ceramide on phosphatidylcholine membranes: a deuterium NMR study, *Biophys. J.* 82 (2002) 3089–3095.
- [42] L. Silva, R.F.M. De Almeida, A. Fedorov, A.P.A. Matos, M. Prieto, Ceramide-platform formation and induced biophysical changes in a fluid phospholipid membrane, *Molec. Membr. Biol.* 23 (2006) 137–148.
- [43] M. Fidorra, L. Duellund, C. Leidy, A.C. Simonsen, L.A. Bagatolli, Absence of fluid-ordered/fluid-disordered phase coexistence in ceramide/POPC mixtures containing cholesterol, *Biophys. J.* 90 (2006) 4437–4451.
- [44] J.M. Holopainen, H.L. Brockman, R.E. Brown, P.K.J. Kinnunen, Interfacial interactions of ceramide with dimyristoylphosphatidylcholine: impact of the N-acyl chain, *Biophys. J.* 80 (2001) 765–775.
- [45] A. Terzaghi, G. Tettamanti, M. Masserini, Interaction of glycosphingolipids and glycoproteins—thermotropic properties of model membranes containing G(M1) ganglioside and glycophorin, *Biochemistry* 32 (1993) 9722–9725.
- [46] A. Ferraretto, M. Pitto, P. Palestini, M. Masserini, Lipid domains in the membrane: thermotropic properties of sphingomyelin vesicles containing GM1 ganglioside and cholesterol, *Biochemistry* 36 (1997) 9232–9236.
- [47] A.G. Lee, Lipid phase-transitions and phase-diagrams. II. Mixtures involving lipids, *Biochim. Biophys. Acta* 472 (1977) 285–344.
- [48] S.A. Pandit, S.W. Chiu, E. Jakobsson, A. Grama, H.L. Scott, Cholesterol surrogates: a comparison of cholesterol and 16:0 ceramide in POPC bilayers, *Biophys. J.* 92 (2007) 920–927.
- [49] A. Tsamaloukas, H. Szadkowska, H. Heerklotz, Nonideal mixing in multicomponent lipid/detergent systems, *J. Phys. Condens. Matter* 18 (2006) S1125–S1138.
- [50] A. Bunge, P. Muller, M. Stockl, A. Herrmann, D. Huster, Characterization of the ternary mixture of sphingomyelin, POPC, and cholesterol: support for an inhomogeneous lipid distribution at high temperatures, *Biophys. J.* 94 (2008) 2680–2690.
- [51] E. Klapisz, J. Maslah, G. Berezziat, C. Wolf, K.S. Koumanov, Sphingolipids and cholesterol modulate membrane susceptibility to cytosolic phospholipase A(2), *J. Lipid Res.* 41 (2000) 1680–1688.
- [52] K.S. Koumanov, P.J. Quinn, G. Berezziat, C. Wolf, Cholesterol relieves the inhibitory effect of sphingomyelin on type II secretory phospholipase A(2), *Biochem. J.* 336 (1998) 625–630.